2022 19th International Conference on Electrical Engineering, Computing Science and Automatic Control (CCE). Mexico City, Mexico. November 9-11, 2022

Nanostructured Films of Bi_2SeO_5 Deposited by Pulsed Laser Ablation

J.A. Melchor-Robles
Doctorado Nanociencias y Nanotecnología, CINVESTAV-IPN. Instituto Politécnico Nacional 2508, San Pedro Zacatenco, Gustavo A. Madero, 07360, Ciudad de México,CDMX.
jairmelchor@gmail.com

Jacobo Martínez-Reyes
Programa de Doctorado Nanociencias y Nanotecnología, CINVESTAV-IPN.. Estancias Posdoctorales Vinculadas al Fortalecimiento de la Calidad del Posgrado Nacional por CONACYT convocatoria 2020
jacobomartinezreyes@gmail.com

Karen Rodriguez-Rosales
Programa de Doctorado en Ciencias de la Energía UAQ. Universidad 231, Cerro de las Campanas S/N, Las Campanas, 76010 Santiago de Querétaro, Qro.
karen.uaq@outlook.com

A. Maldonado-Álvarez
Departamento de Ingeniería Eléctrica-SEES. CINVESTAV-IPN. Av. Instituto Politécnico Nacional 2508, San Pedro Zacatenco, Gustavo A. Madero, 07360, Ciudad de México,CDMX.
amaldo@cinvestav.mx

Francisco Javier de Moure Flores
Departamento de posgrado en Ciencias de la Energía. Universidad 231, Cerro de las Campanas S/N, Las Campanas, 76010 Santiago de Querétaro, Qro
fcomoure@hotmail.com

María de la Luz Olvera-Amador
Departamento de Ingeniería Eléctrica-SEES. CINVESTAV-IPN. Instituto Politécnico Nacional 2508, San Pedro Zacatenco, Gustavo A. Madero, 07360, Ciudad de México,CDMX.
molvera@cinvestav.mx

***Abstract*— Nanostructured Bi_2SeO_5 films were deposited on soda-lime glass substrates by the pulsed laser ablation technique, PLA, using a target manufactured from powders synthesized by solid-state reaction, starting from a stoichiometric mixture of the precursors, Bi_2O_3 and Se. The films, with a thickness of 250 nm and subsequent heat treatment at 550 and 600 °C, present a flake-like nanostructured morphology. From the indexing of the X-ray diffractogram, the obtaining of an orthorhombic structure is confirmed. Morphological characterization was performed using SEM and AFM microscopy. The flake-shaped particles presented thicknesses between 20 and 30 nm and the average roughness measured was 15 nm. From the UV-Vis transmittance spectra, average optical transmittances were obtained in the visible region of the order of 60 % and bandgap magnitudes of 3.3 to 3.7 eV were estimated.**

Keywords*— *Oxicalcogenuros, Bi_2SeO_5, transparent semiconductors, PLA.

I. INTRODUCTION

The electronics industry massively generates products based on semiconductor materials for multiple final applications, such as mobile devices for 5G communication, electrical vehicles, autonomous systems, and LoT (Smart city, Smart home and industrial) devices, among others [1]. Recently, the chains that supply semiconductors to the industry suffered a 40 % reduction in production; causing a shortage of chips, along with the reduction of the annual growth of the sector from 12.5 to 0.9%, negatively impacting sales and production in economic areas, such as smartphones (-2.5%), PCs & tablets (-5.8%), automotive sector (-24.0%), and other [2–6].

Based on the problem identified, it is necessary to carry out researchs related to the synthesis, characterization and evaluation of new materials for the semiconductor industry. One of the fields that is currently of great interest is chalcogenide materials, such as rare earth sulfides, selenides, and oxides of chalcogenides. Its derivatives, such as binary, ternary, and quaternary chalcogenide materials, are applicable in many areas, as is the case of photovoltaics, photocatalysis, sensors, fuel cells, and batteries, to name a few [7–9]. One of the most promising systems, due to its dual properties, is the BiCuOSe oxychalcogenide. This presents a p-type semiconducting conductivity, theoretically a variable band gap varying between 1.1 to 3.5 eV [10–12], low carrier concentration has been reported, and by doping it exhibits a moderate electrical resistivity and low thermal conductivity [13-14].

Within the characteristic polymorphism of BiCuOSe we find bismuth oxy-selenide (Bi_2O_2Se), a two-dimensional semiconductor with high electron mobility [15–17], when in contact with air it thermally oxidizes to form bismuth dibismuth selenium pentoxide (Bi_2SeO_5), which has a high dielectric constant and therefore insulating properties [18–22]. Recently, semiconducting Bi_2O_2Se layered material has been synthesized, exhibiting thickness dependent band gap and airs stability. Controlled oxidation of Bi2O2Se layers and facile etching of Bi_2SeO_5 a time-dependent oxidation of Bi_2O2Se, showing a linear relationship between the sample thickness and oxidation time [23].

The Bi_2SeO_5, is of scientific interest due to its acentric crystallization of the Abm2 space group, favoring the formation of distorted pyramids [24]. The theoretical models obtained required the disorder of at least three atoms of the selenite group, favoring the transition from Bi_2O_2Se to Bi_2SeO_5 in the centrosymmetrics of the space group Abmm (No.67), indicating a heterojunction type formation [25]. Bi_2SeO_5 is one of the simplest Aurivillius oxides, it has excellent dielectric properties and nonlinear optical effects, with a reported band gap greater than 3 eV [16], [26].

Based on the above, in the present work nanostructured Bi_2SeO_5 thin films were synthesized, deposited by means of the pulsed laser technique, PLA, using a target made from Bi_2SeO_5 powders, synthesized by mechanical grinding of the precursors, Bi_2O_3 and Se. Likewise, the results of the structural, morphological, and optical characterization of the films are presented.

II. EXPERIMENTAL METHODOLOGY

Synthesis process

Bi_2SeO_5 polycrystalline systems were synthesized from the precursor powders with a 1:1 stoichiometric ratio, for which the following reagents were used: Se (99.5%, Sigma Aldrich) and Bi_2O_3 (99.9%, Sigma Aldrich). The synthesis of the material was carried out by mechanical grinding, using a PULVERISETTE 7 planetary ball mill. The powders were ground for 8 h, clockwise and counterclockwise at 400 revolutions per minute (rpm) with a ball/powder weight ratio of 10:1. Once the grinding process was finished, 6 g of the obtained powder **were** weighed on an analytical balance and then placed in a mechanical die to make a 7 mm diameter and 4 mm thick pellet. A hydraulic pressing machine with a pressure of 15 tons was used to obtain mechanically stable pellets, which were later used as targets for pulsed laser deposition (PLA). The deposition of the thin films by PDL was carried out in a vacuum chamber, at a pressure of 0.1 mTorr and a 1064 nm laser. The target-substrate distance was set at 60 mm. The deposition time was 5 min. After the deposit of the films, they were subjected to a thermal treatment in a flow of high purity N_2 with a flow of 5 L/min at two different temperatures, 550 and 600°C, for 60 min. In what follows the samples will be identified as, Bi_2SeO_5-550 and Bi_2SeO_5-600.

Characterization Techniques

Crystal structure analysis was performed with a PANalytical model X-Pert Pro diffractometer, using the Cu-Kα emission source, λ_{Cu} = 0.154178 nm, with a voltage of 45 KV and a electrical current of 40 mA, scanning the angle 2θ from 20 to 75 °, and a step of 0.02 ° degrees per minute. Phase analysis was performed using Panalytical's High Score Plus software, from the International Center for Diffraction Data, ICDD database.

The morphology of the systems was characterized by high resolution scanning electron microscopy, SEM, in a JEOL JSM-7401F equipment. The voltage used to analyze the sample was kept in the range of 18 to 25 kV, with an electrical current of 15 nA. The elemental chemical analysis of the samples was performed by Energy Dispersive Spectroscopy, EDS. Additionally, to analyze the morphology of the surface and the uniformity of the films deposited by PLA, 2 and 3D images were obtained and the surface roughness was measured by atomic force microscopy, AFM. The AFM equipment used was a microscope of the NT-MDT Spectrum Instruments brand, using the semi-contact mode.

The optical transmittance, the proportion of light that samples allow to pass with respect to the intensity of the incident light, was measured through the ultraviolet-visible, UV-Vis, spectroscopy technique, which was carried out with a Jasco-670 equipment in an interval of 200 to 1100 nm, with a step of 1 nm.

Finally, using a JEM-ARM200F transmission electron microscope (TEM) it was possible to obtain the electron diffraction patterns.

III. RESULTS AND DISCUSSION

Thin film Bi_2SeO_5

Figure 1 shows the physical appearance of one of the deposited Bi_2SeO_5 films, with dimensions of 3 cm x 4 cm (Figure 1A); all samples were optically transparent (Figure 1B).

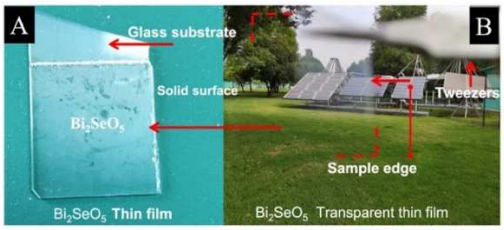

Fig 1. *(A) Photograph of the Bi_2SeO_5 thin film with dimensions 3 cm x 4 cm, (B) Image showing the transparency of the Bi_2SeO_5 films.*

X-ray diffraction

The diffraction patterns of the Bi_2SeO_5 films thermally treated at 550 and 600 °C, and the diffraction pattern given in the ICCD-PDF letter # 96-810-0905 by the ICDD for the same compound, are shown in the figure 2A. From the spectra it can be seen that both films show the main diffraction peaks of the Bi_2SeO_5 phase. The characteristic peaks of the material in 2θ the angles, 27.9, 32.6, 33.2, 46.1, 53.6 and 55.9° correspond to the Miller indices (231), (002), (402), (460), (631), and (291), respectively. From these spectra, the crystallite size (1), interplanar spacing (2), dislocation densities (3) and strain (4), was estimated for the preferential peak with Miller indices (231).

$$D = 0.9\,\lambda/\beta\cos\theta \quad (1)$$

$$d = n\lambda/2\sin\theta \quad (2)$$

$$\delta = 1/D^2 \quad (3)$$

$$\varepsilon = \beta/4tan\theta \quad (4)$$

Where λ is the wavelength of the radiation used, β is the full width at half maximum (FWHM) of the peak, n is the diffraction order and θ is the angle of the diffraction peak with Miller indices (hkl).

TABLE 1. *The calculated crystallite parameters from XRD studies; crystallite sizes, interplanar distance, dislocation densities, and strain.*

Sample	FWHM (degrees)	Interplanar distance, d	Crystallite size, D [nm]	Microstrain, ε, (10^{-3})	Dislocation density, δ (10^{-4})
Bi_2SeO_5-550	0.64	3.19	13.35	-2.85	56.09
Bi_2SeO_5-600	0.40	3.18	20.94	-1.81	22.80

Based on the values reported in Table 1, it was possible to identify that the thin film of Bi_2SeO_5-600 presents better results after the annealing treatment, increasing its crystallite size, approaching a greater interplanar distance compared to that reported in the ICCD-PDF, in addition, strain in the film was identified due to defects close to zero and a lower value in the density of dislocations that was associated with the polycrystalline of the sample.

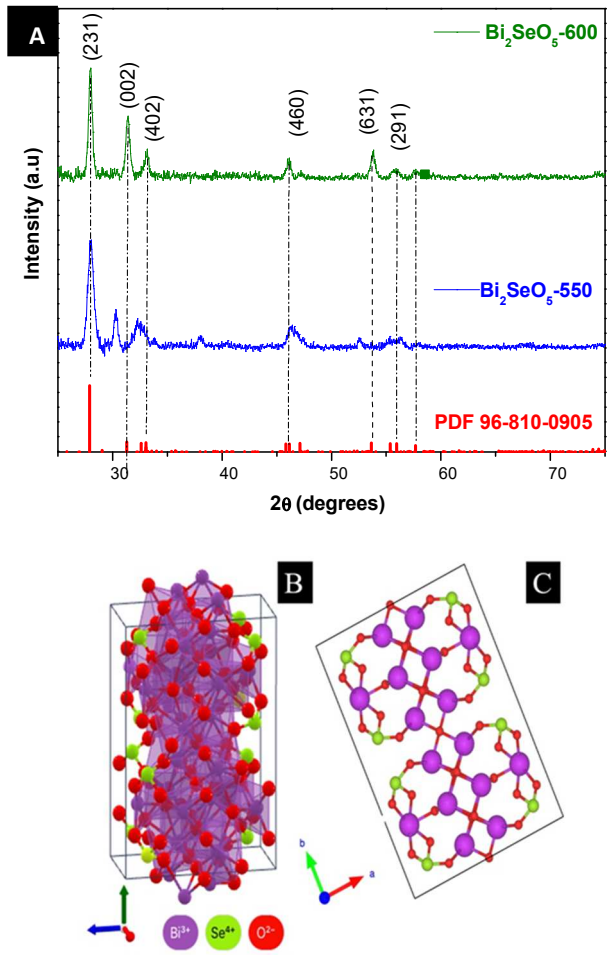

Fig 2. *(A) Diffraction patterns of Bi_2SeO_5-ICDD-PDF # 96-810-0905, Bi_2SeO_5-550, and Bi_2SeO_5-600. (B) Bi_2SeO_5 orthorhombic primitive cell. (C) Crystallographic plane with Miller indices (231).*

The crystallographic system of the Bi_2SeO_5 obtained corresponds to an orthorhombic structure (Figure 2B). The structure presents a space group 39-Abm2, with a point group mm2, lattice parameters a=11.42 Å, b=16.24 Å, c=5.48 Å, and a cell volume of 1018.32 106 pm3. Figure 2C shows the atomic structure of the (231) preferential plane [27]. These crystallographic data are consistent with those theoretically reported by Rademacher et al. [24].

Bi_2SeO_5 polycrystalline systems, reported by Tu et al., [20] show a gradual and selective oxidation process of the system, forming an amorphous crystalline structure. Likewise, Peng et al.,[16] reported the study of dielectric properties of the material using thicknesses of 20 nm of the Bi_2O_2Se systems as well as roughness studies based on its oxidation.

On the other hand, Liang et al.[27] reported that the characteristic peaks of Bi_2SeO_5 with an orthorhombic structure and the main peak at (231) corresponds to the JCPDS:70-5102 chart, also indicating that no clear diffraction peaks were observed for impurities such as selenites of bismuth, bismuth oxide or selenium oxide. Furthermore, in that work it is considered that the Bi_2SeO_5 phase is metastable in the range of 300 to 600 ºC. Dityatyev et al. conclude that the phase of Bi_2SeO_5 is due to its order-disorder transition nature that predominantly involves the reorientation of the SeO_3 group [25].

Scanning electron microscopy (SEM), and Energy Dispersive Spectroscopy (EDX)

The surface of the Bi_2SeO_5 thin films is covered with ordered figures distributed in intercalated layers (Figure 3A-C), on which nanoflake-type shapes stand out (Figure 3B), with an average grain size of 53 nm and a height and length of 200 and 600 nm, respectively. These characteristics could suggest that the deposition process allowed the upward growth of the system from dimension 0 to form a 3D nanostructure (Figure 3D), thus leading to the formation of a textured surface, or preferential deposition.

This type of growth is derived from the solidification process that would correspond to the BCF (Burton Cabrera-Frank) model, where growth on the surface, or in volume, is due to non-equilibrium conditions, that imply the displacement of monatomic steps by diffusion of atoms and incorporation of others, in addition to identifying that the crystal dislocations contain a helical or screw component due to the spiral surface formed by the atomic planes around the dislocation line (Figure 3E) [28-29].

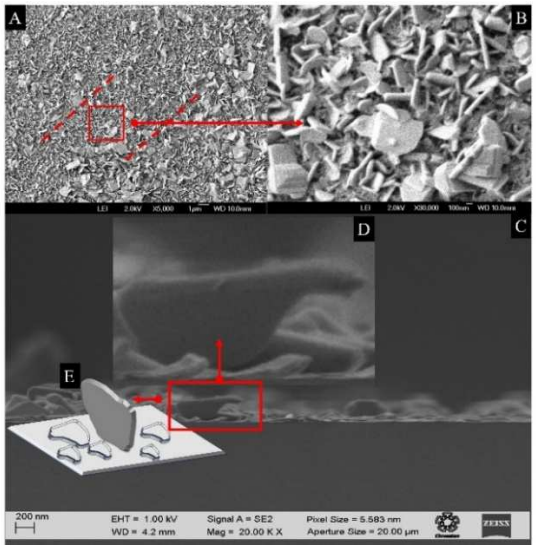

Fig 3. *A) Bi_2SeO_5-550 thin film surface, B) Flake-like morphology, C) Perpendicular section of the thin film, D) Nanoflake-like crystal, E) Preferential growth model of nanoflakes.*

Comparing the morphology obtained with other reported works, Liang [27] reported a morphology corresponding to irregular nanosheets of Bi_2Se_3. When sample is calcined at 300 ºC, the system forms the Bi_2SeO_5 phase with the presence of irregular sheets stacked in the form of microspheres, or nano type-flowers with calcination at 500 ºC, depending on the temperature range. In our case, we were able to identify that by increasing the calcination temperature to 600 ºC, the Bi_2SeO_5 presents transition zones, where it is possible to observe homogeneity of the material due to the formation of a metastable phase, as well as filaments of ~ 4 mm in length and thickness of ~150 nm, in addition to agglomerates and particles (Figure 4A). This result indicates that the calcination temperature is too high to decompose the microspheres or, in this case, the nanoflakes; a phenomenon also observed by Liang (Figure 4B). In the microstructure, staggered deposits with agglomerates of regular nanoparticles of ∽30 nm (Figure 4A) and the generation of porosity on the material matrix are visualized (Figure 4B).

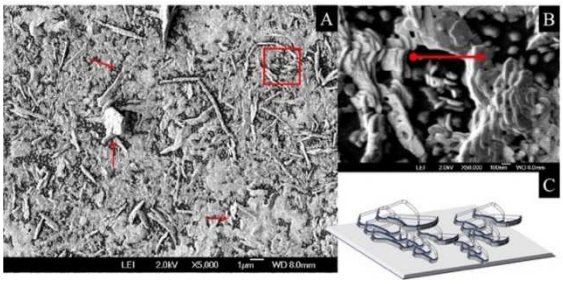

Fig 4. *A) Bi_2SeO_5 thin film surface thermally treated at 600 ºC, B) Flake-like morphology, C) Growth Pattern (BCF).*

From the EDS results, it can be seen that the system treated at 550 ºC shows a quasi-homogeneous distribution of elements (Figure 5A) due to the evaporation process during the deposition by **PLA** and the mechanism that leads to the ablation of the material, depending on the intensity of the laser and the topology of the material. Elemental peaks Bi (28.11% Wt), O (3.57% wt) and Se (5.96% wt) predominate in the sample (Figure 5B), and the generation of an alloying system can be observed. Additionally, some other elements, such as Ca, Na and Si, coming from the glass substrate are evidenced (Figure 5C) [29].

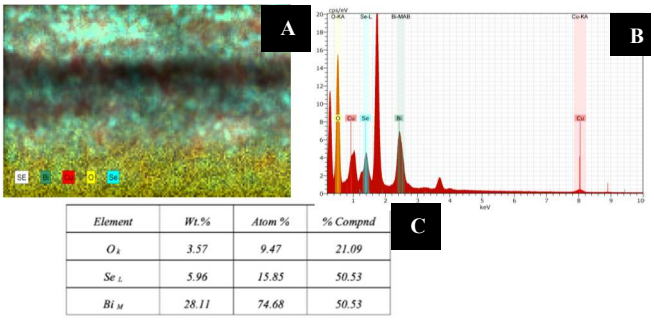

Element	Wt.%	Atom %	% Compnd
O_K	3.57	9.47	21.09
Se_L	5.96	15.85	50.53
Bi_M	28.11	74.68	50.53

Fig 5. *A) Mapping of the Bi_2SeO_5-550 sample, B) Energy dispersive spectrum, EDS, C) Quantitative analysis of the composition.*

For the Bi_2SeO_5-600 sample, the composition mapping shows the predominance of Se (Figure 6A), based on the local analysis (Figure 6B), the distribution between the elements Se (13.57 %Wt), Bi (54.92 %Wt) and O (27.01%Wt) shows the strong Se-O relationship due to the fragmentation caused by the calcination process and the increase in the distribution of the free Bi element on the surface. This may be due to the influence of the thermal gradient. This assertion was corroborated through a thermogravimetric analysis by Dityatyev et al. [25], and a possible disorder is suggested from 600 ºC, identifying that the selenite group, SeO_3, begins to disorder due to high temperatures, generating displacements or exchange of O.

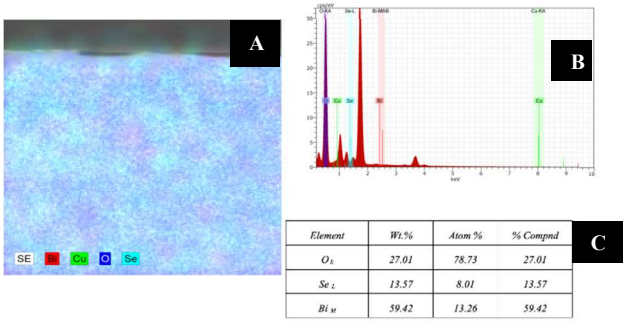

Element	Wt.%	Atom %	% Compnd
O_K	27.01	78.73	27.01
Se_L	13.57	8.01	13.57
Bi_M	59.42	13.26	59.42

Fig 6. *A) Mapping of the composition of the Bi_2SeO_5 sample thermally treated at 600 ºC, B) Dispersive energy spectrum, EDS, C) Quantitative analysis of the composition.*

Atomic force microscopy, AFM

The analysis of the surface morphology was complemented with atomic force microscopy, AFM. Figure 7A shows the surface of the Bi_2SeO_5-550 sample with a scanning area of 5 µm x 5 µm. Figures nanoflakes-type with maximum height around of 180 nm are observed in it (Figure 7B). The average roughness estimated is of 15.25 nm, evidencing that the sample has a possible crystallographic texture or preferential orientation based on nano flakes that make up the thin film on the surface.

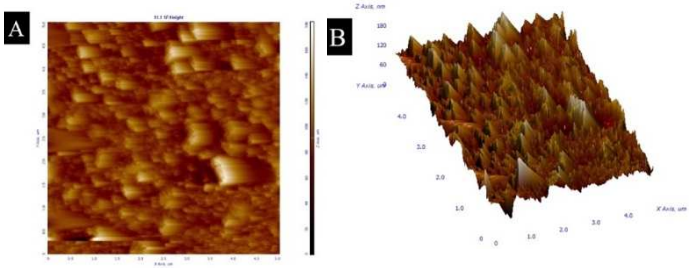

Fig 7. *Images of the surface morphology of the Bi_2SeO_5-550 sample. A) 2D image, B) 3D image.*

The Bi_2SeO_5-600 system exhibits stacking plates with average dimensions of 100 to 150 nm in a 4.5 µm x 4.5 µm scanning section (Figure 8A), evidencing that the thermal treatment fragmented the nanoflakes, forming irregular regions in a process to the formation of a new alloy. The average roughness of the sample surface is 18.17 nm (Figure 8B), with a height of 200 nm. In this regard, Li et al., [16], consider that in calcination processes or thermal treatments at temperatures above 400 ºC, accelerated oxidation is favored, identifying the formation of thicker oxide layers. In our case, we observed the fragmentation of the nanoflakes and the formation of stacks of blocks or layers with an average size of 100 to 150 nm.

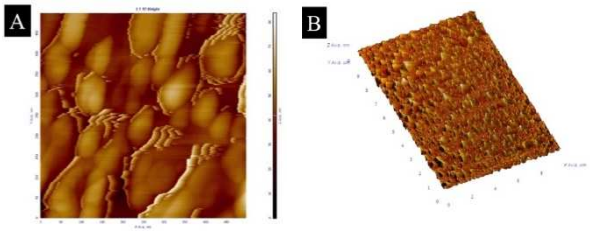

Fig 8. *Images of the surface morphology of the Bi_2SeO_5-600 sample. A) 2D image, B) 3D image.*

UV-Vis Spectrometry

Figure 9 presents the optical transmission spectra of the Bi_2SeO_5 systems in the wavelength range of 250-1200 nm. Using the transmittance values (%) only of the region of the visible spectrum (400 to 700 nm), the intensity that each thin film allows to pass was averaged; in the Bi_2SeO_5-550 film (Figure 9A) the average transmittance reaches values of the order of 50%, while in the Bi_2SeO_5-600 sample (Figure 9B) it is greater than 70%. This result is attributed to the better crystalline quality of this film, also reflected in the X-ray diffractogram. The absorption edges are observed at 330 nm.

From the transmittance spectra, the magnitudes of the bandgap energies were estimated using the Tauc´s method, and the estimated values were, 3.3 and 3.75 eV, for the Bi_2SeO_5-550 and Bi_2SeO_5-600 samples (Figure 9), respectively.

The bandgap energy reported in the literature for the Bi_2SeO_5 system corresponds to an absorption edge ~330 nm, with a value of 3.75 eV, calculated by the Tauc´s method as well [28], [30]. There are other studies that report other values that range from 2.83 to 3.9 eV [22], [26], [28].

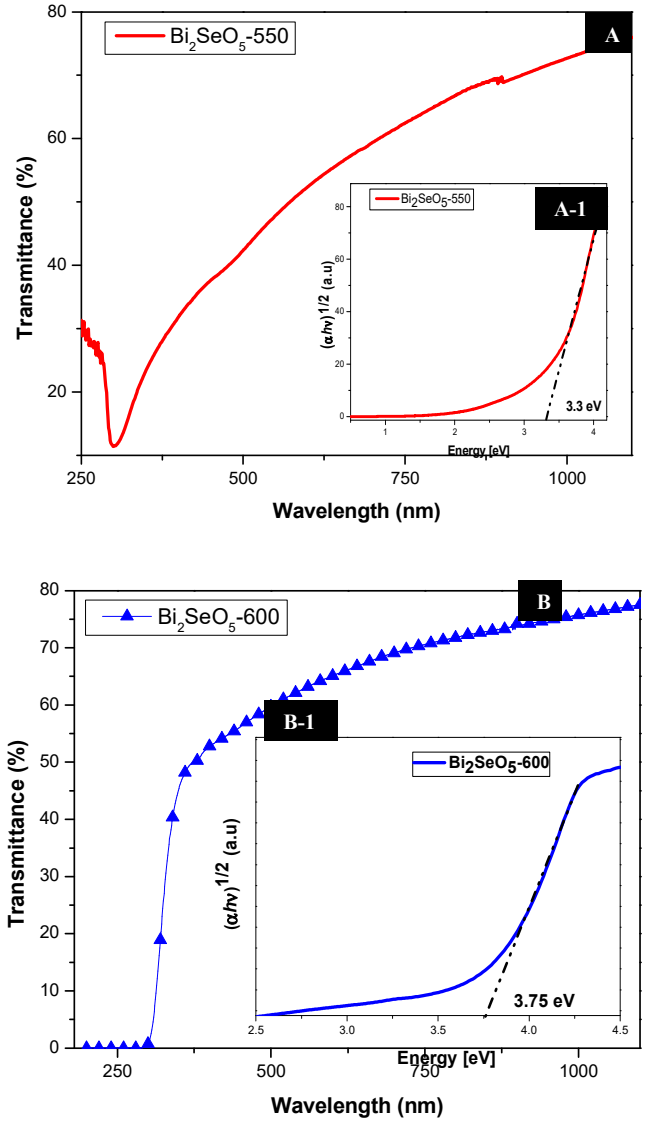

Fig 9. *UV-Vis transmittance spectra of the Bi_2SeO_5 films and estimation of the forbidden band width by the Tauc method. A-1) Bi_2SeO_5-550, B-1) Bi_2SeO_5-600.*

High Resolution Transmission Electron Microscopy, HRTEM

Figure 10 shows the electron diffraction patterns of the synthesized samples, Bi_2SeO_5-550, Bi_2SeO_5-600, obtained by High Resolution Transmission Electron Microscopy. It is observed that the patterns correspond to a polycrystalline material, with planes identified with the structure Bi_2SeO_5, ICCD -PDF # 96-810-0905, with reflections at (231), (002), (402), (460), (631), (291) (Figure 10A-1 and B-1).

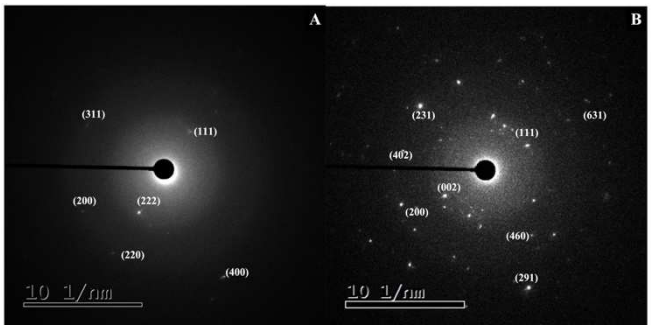

Fig 10. *HRTEM analysis, diffraction patterns of the samples. A) shows Bi_2SeO_5-550, B) Bi_2SeO_5-600.*

IV. CONCLUSIONS

Transparent Bi_2SeO_5 thin films were deposited using the PLA technique on soda-lime glass substrates, with a thickness of the order of 250 nm. The thin films present an orthorhombic structure with a space group Abm2 (39), a point group mm2, and a preferential orientation along the (231) plane, located at 2θ= 27.9°. After performing heat treatments at 550 and 600 °C, the materials show a nanoflake-like morphology with an average thickness of 53 nm, and as the temperature of the heat treatment increases, they collapse, forming a heterogeneous surface with nanofilaments. The Bi_2SeO_5 sample treated at 600 ºC presented a band gap of ∽ 3.7 eV calculated by the Tauc´s method and a transparency greater than 70 % in the visible spectrum region with a absorption edge near 330 nm.

The Bi_2SeO_5-550 system presents a possible texture of nano flakes derived from the solidification process. The nanoflakes have an average height of 200 nm and a roughness of 15.25 nm, measured by AFM. The influence of roughness in thin films is associated with a higher transmittance.

Based on the experimental results obtained, the general properties of Bi_2SeO_5 thin films can be recommended for their use in the fabrication of semiconductor devices, or as catalysts for the degradation of organic pollutants and/or the development of sensors.

AKNOWLEDGMENTS

Jacobo Martínez-Reyes thank the economical support received from “Estancias Posdoctorales Vinculadas al Fortalecimiento de la Calidad del Posgrado Nacional por CONACYT, convocatoria 2020 (1)”.

Authors also want to appreciate the technical support from M.A Luna Arias, A. Tavira Fuentes, Georgina Ramirez, Marcela Guerrero, Ángel Guillen, Daniel Bahena, and J. Roque (CINVESTAV-IPN). Jair A. Melchor Robles acknowledges to CONACYT-México for the scholarship received during PhD Nanosciences and Nanotechnology studies at Cinvestav-IPN, Mexico.

REFERENCES

[1] Michaela D. Platzer, Karen M. Sutter, and John F. Sargent Jr., “Semiconductors:U.S.Industry, Global Competition, and Federal Policy. ,” Oct. 2020.

[2] X. Wu, C. Zhang, and W. Du, “An Analysis on the Crisis of ‘Chips shortage’ in Automobile Industry ——Based on the

Double Influence of COVID-19 and Trade Friction," *J Phys Conf Ser*, vol. 1971, no. 1, p. 012100, Jul. 2021, doi: 10.1088/1742-6596/1971/1/012100.

[3] Harald Bauer, Ondrej Burkacky, Peter Kenevan, Abhijit Mahindroo, and Mark Patel, "Coronavirus: Implications for the semiconductor industry. Mckinsey & Company," Apr. 2020.

[4] M. Cai and J. Luo, "Influence of COVID-19 on Manufacturing Industry and Corresponding Countermeasures from Supply Chain Perspective," *J Shanghai Jiaotong Univ Sci*, vol. 25, no. 4, pp. 409–416, Aug. 2020, doi: 10.1007/s12204-020-2206-z.

[5] Y. Song, X. Hao, Y. Hu, and Z. Lu, "The Impact of the COVID-19 Pandemic on China's Manufacturing Sector: A Global Value Chain Perspective," *Front Public Health*, vol. 9, May 2021, doi: 10.3389/fpubh.2021.683821.

[6] M. A. Dar, B. Gladysz, and A. Buczacki, "Impact of COVID19 on Operational Activities of Manufacturing Organizations—A Case Study and Industry 4.0-Based Survive-Stabilise-Sustainability (3S) Framework," *Energies (Basel)*, vol. 14, no. 7, p. 1900, Mar. 2021, doi: 10.3390/en14071900.

[7] E. Y. Muslih, B. Munir, and M. M. Khan, "Advances in chalcogenides and chalcogenides-based nanomaterials such as sulfides, selenides, and tellurides," in *Chalcogenide-Based Nanomaterials as Photocatalysts*, Elsevier, 2021, pp. 7–31. doi: 10.1016/B978-0-12-820498-6.00002-0.

[8] N. Anscombe, "The promise of chalcogenides," *Nat Photonics*, vol. 5, no. 8, pp. 474–474, Aug. 2011, doi: 10.1038/nphoton.2011.155.

[9] Zakery, "An Introduction to Chalcogenide Glasses," in *Optical Nonlinearities in Chalcogenide Glasses and their Applications*, Zakery A, Ed. Berlin, Heidelberg: Springer Berlin Heidelberg, pp. 1–28. doi: https://doi.org/10.1007/978-3-540-71068-4_1.

[10] A. P. Richard, J. A. Russell, A. Zakutayev, L. N. Zakharov, D. A. Keszler, and J. Tate, "Synthesis, structure, and optical properties of BiCuOCh (Ch=S, Se, and Te)," *J Solid State Chem*, vol. 187, pp. 15–19, Mar. 2012, doi: 10.1016/j.jssc.2011.11.013.

[11] L. Pan *et al.*, "Realization of n-type and enhanced thermoelectric performance of p-type BiCuSeO by controlled iron incorporation," *J Mater Chem A Mater*, vol. 6, no. 27, pp. 13340–13349, 2018, doi: 10.1039/C8TA03521K.

[12] R. Woods-Robinson *et al.*, "Wide Band Gap Chalcogenide Semiconductors," *Chem Rev*, vol. 120, no. 9, pp. 4007–4055, May 2020, doi: 10.1021/acs.chemrev.9b00600.

[13] L. D. Zhao, D. Berardan, Y. L. Pei, C. Byl, L. Pinsard-Gaudart, and N. Dragoe, "Bi1−xSrxCuSeO oxyselenides as promising thermoelectric materials," *Appl Phys Lett*, vol. 97, no. 9, p. 092118, Aug. 2010, doi: 10.1063/1.3485050.

[14] Y. Yu, M. Cagnoni, O. Cojocaru-Mirédin, and M. Wuttig, "Chalcogenide Thermoelectrics Empowered by an Unconventional Bonding Mechanism," *Adv Funct Mater*, vol. 30, no. 8, p. 1904862, Feb. 2020, doi: 10.1002/adfm.201904862.

[15] T. Li and H. Peng, "2D Bi $_2$ O $_2$ Se: An Emerging Material Platform for the Next-Generation Electronic Industry," *Acc Mater Res*, vol. 2, no. 9, pp. 842–853, Sep. 2021, doi: 10.1021/accountsmr.1c00130.

[16] T. Li *et al.*, "A native oxide high-κ gate dielectric for two-dimensional electronics," *Nat Electron*, vol. 3, no. 8, pp. 473–478, Aug. 2020, doi: 10.1038/s41928-020-0444-6.

[17] J. Wu *et al.*, "Low Residual Carrier Concentration and High Mobility in 2D Semiconducting Bi $_2$ O $_2$ Se," *Nano Lett*, vol. 19, no. 1, pp. 197–202, Jan. 2019, doi: 10.1021/acs.nanolett.8b03696.

[18] M. Kang *et al.*, "Low-Temperature and High-Quality Growth of Bi $_2$ O $_2$ Se Layered Semiconductors *via* Cracking Metal–Organic Chemical Vapor Deposition," *ACS Nano*, vol. 15, no. 5, pp. 8715–8723, May 2021, doi: 10.1021/acsnano.1c00811.

[19] Q. Wei *et al.*, "Physics of intrinsic point defects in bismuth oxychalcogenides: A first-principles investigation," *J Appl Phys*, vol. 124, no. 5, p. 055701, Aug. 2018, doi: 10.1063/1.5040690.

[20] T. Tu *et al.*, "Uniform High-k Amorphous Native Oxide Synthesized by Oxygen Plasma for Top-Gated Transistors," *Nano Lett*, vol. 20, no. 10, pp. 7469–7475, Oct. 2020, doi: 10.1021/acs.nanolett.0c02951.

[21] C. Liu, P. Wang, Y. Qiao, and G. Zhou, "Self-assembled Bi2SeO5/rGO/MIL-88A Z-scheme heterojunction boosting carrier separation for simultaneous removal of Cr (VI) and chloramphenicol," *Chemical Engineering Journal*, vol. 431, p. 133289, Mar. 2022, doi: 10.1016/j.cej.2021.133289.

[22] Y. Yu. Illarionov, T. Knobloch, and T. Grasser, "Native high-k oxides for 2D transistors," *Nat Electron*, vol. 3, no. 8, pp. 442–443, Aug. 2020, doi: 10.1038/s41928-020-0464-2.

[23] H. Li, X. Xu, Y. Zhang, R. Gillen, L. Shi, and J. Robertson, "Native point defects of semiconducting layered Bi2O2Se," *Sci Rep*, vol. 8, no. 1, p. 10920, Dec. 2018, doi: 10.1038/s41598-018-29385-8.

[24] O. Rademacher, H. Göbel, M. Ruck, and H. Oppermann, "Crystal structure of dibismuth selenium pentoxide, Bi2SeO5," *Zeitschrift für Kristallographie - New Crystal Structures*, vol. 216, no. 1–4, pp. 29–30, Apr. 2001, doi: 10.1524/ncrs.2001.216.14.29.

[25] O. A. Dityatyev, P. Smidt, S. Y. Stefanovich, P. Lightfoot, V. A. Dolgikh, and H. Opperman, "Phase equilibria in the Bi2TeO5□Bi2SeO5 system and a high temperature neutron powder diffraction study of Bi2SeO5," *Solid State Sci*, vol. 6, no. 9, pp. 915–922, Sep. 2004, doi: 10.1016/j.solidstatesciences.2004.05.004.

[26] T. Cheng, C. Tan, S. Zhang, T. Tu, H. Peng, and Z. Liu, "Raman Spectra and Strain Effects in Bismuth Oxychalcogenides," *The Journal of Physical Chemistry C*, vol. 122, no. 34, pp. 19970–19980, Aug. 2018, doi: 10.1021/acs.jpcc.8b05475.

[27] S. Liang, J. Wang, X. Wu, S. Zhu, and L. Wu, "Phase transformation synthesis of a new Bi2SeO5 flower-like microsphere for efficiently photocatalytic degradation of organic pollutants," *Catal Today*, vol. 327, pp. 357–365, May 2019, doi: 10.1016/j.cattod.2018.03.021.

[28] M. Tang, Y. Ao, P. Wang, and C. Wang, "All-solid-state Z-scheme WO3 nanorod/ZnIn2S4 composite photocatalysts for the effective degradation of nitenpyram under visible light irradiation," *J Hazard Mater*, vol. 387, p. 121713, Apr. 2020, doi: 10.1016/j.jhazmat.2019.121713.

[29] Burton K, "The growth of crystals and the equilibrium structure of their surfaces," *Philosophical Transactions of the Royal Society of London. Series A, Mathematical and Physical Sciences*, vol. 243, no. 866, pp. 299–358, Jun. 1951, doi: 10.1098/rsta.1951.0006.

[30] H. Li, J. Li, Z. Ai, F. Jia, and L. Zhang, "Oxygen Vacancy-Mediated Photocatalysis of BiOCl: Reactivity, Selectivity, and Perspectives," *Angewandte Chemie International Edition*, vol. 57, no. 1, pp. 122–138, Jan. 2018, doi: 10.1002/anie.201705628.